Nonlinear Effects on Convectively Forced Two-Dimensional Mesoscale Flows

JI-YOUNG HAN* AND JONG-JIN BAIK

School of Earth and Environmental Sciences, Seoul National University, Seoul, South Korea

(Manuscript received 14 December 2011, in final form 12 June 2012)

ABSTRACT

One of the important problems in mesoscale atmospheric dynamics is how the atmosphere responds to convective heating or cooling. Here, the authors examine nonlinear effects on convectively forced mesoscale flows in the context of the nonlinear response of a stably stratified flow to elevated steady heating in two dimensions using a nondimensional numerical model. Results of two-dimensional numerical experiments in a uniform flow show that even without vertical wind shear, a separation of an upwind cellular updraft from the steady heating-induced main updraft occurs in a highly nonlinear flow system. This separation occurs as the compensating cellular downdraft associated with a secondary maximum in the main updraft develops. As the nonlinearity of the flow system increases, the upwind cellular updraft is separated earlier and becomes stronger. Smaller viscous terms result in the separation of more cellular updrafts, which become stronger and move farther away from the main updraft region. In particular, in an inviscid flow, cellular updrafts are periodically separated from the main updraft, and the first cellular updraft and downdraft have intensities comparable to the intensity of the main updraft. In a viscid flow with a constant vertical wind shear up to a certain height, the propagating cellular updraft and downdraft are produced when the nonlinearity is large, as in a uniform flow. Stronger vertical wind shear leads to the earlier formation of the cellular updraft and its stronger intensity, faster propagating speed, and longer lifetime. Results of numerical experiments with squall line–type forcing imply that the highly nonlinear state is necessary for the development of cellular updrafts.

1. Introduction

The basic dynamics of thermally forced mesoscale flows can be understood by examining the linear response of a stably stratified flow to specified diabatic forcing theoretically (e.g., Olfe and Lee 1971; Lin and Smith 1986; Han and Baik 2009, 2010). However, without considering nonlinear effects, some features observed in strong convective systems cannot be explained. For example, the feature of cellular vertical velocity fields in squall lines is attributed to the nonlinear dynamics (Pandya and Durran 1996). One of the analytical methods used to investigate the effects of nonlinearity on thermally forced flows is to solve a weakly nonlinear problem using the perturbation method (Chun and Baik 1994; Baik and Chun 1997; Chun 1997). Another method is to transform the equations of momentum and thermodynamics into conservative forms by assuming that the heat source is proportional to the vertical velocity in a steady-state, inviscid flow system (e.g., Moncrieff and Green 1972; Moncrieff and Miller 1976; Moncrieff 1978). In this method, the heat source can modify but not induce internal gravity waves (Smith and Lin 1982).

Solving a fully nonlinear problem with specified diabatic forcing would be the best way to understand the role of nonlinearity in the dynamics of thermally forced mesoscale flows. However, it appears to be very difficult to obtain analytic solutions for a fully nonlinear system with specified diabatic forcing. Thus, as an alternative way to examine the fully nonlinear response of the flow to diabatic forcing, simple nonlinear numerical models were used in several studies (e.g., Raymond and Rotunno 1989; Baik and Chun 1996; Chun et al. 2008). As an example, a nondimensional model, which simplifies the problem by reducing the number of parameters and combining them into some useful nondimensional parameters (Grant 2000), was developed by Baik and Chun (1996) to investigate the effects of nonlinearity on

* Current affiliation: Korea Institute of Atmospheric Prediction Systems, Seoul, South Korea.

Corresponding author address: Jong-Jin Baik, School of Earth and Environmental Sciences, Seoul National University, Seoul 151-742, South Korea.
E-mail: jjbaik@snu.ac.kr

DOI: 10.1175/JAS-D-11-0335.1

the flow response to low-level heating in a uniform flow. Using the same model but with different diabatic forcing and basic-state wind profile, Chun et al. (2008) investigated nonlinearity effects on convectively forced internal gravity waves and proposed a way to include a nonlinear forcing effect in a convective gravity wave drag parameterization.

In this study, the role of nonlinearity in convective heating–induced flows with and without basic-state vertical wind shear is examined using the nondimensional numerical model developed by Baik and Chun (1996). For this purpose, a series of numerical experiments with various degrees of nonlinearity of the flow system are performed. The nondimensional model and experimental design are described in section 2. Experimental results are presented and discussed in section 3. A summary and conclusions are given in section 4.

2. Nondimensional model

Equations for two-dimensional motion in a hydrostatic, nonrotating, Boussinesq atmosphere with thermal forcing can be expressed by

$$\frac{\partial u}{\partial t} + (U+u)\frac{\partial u}{\partial x} + w\frac{\partial u}{\partial z} + w\frac{dU}{dz} = -\frac{\partial \pi}{\partial x} - \nu u, \quad (1)$$

$$\frac{\partial \pi}{\partial z} = b, \quad (2)$$

$$\frac{\partial b}{\partial t} + (U+u)\frac{\partial b}{\partial x} + w\frac{\partial b}{\partial z} + N^2 w = \frac{g}{c_p T_0} q - \nu b, \quad \text{and} \quad (3)$$

$$\frac{\partial u}{\partial x} + \frac{\partial w}{\partial z} = 0, \quad (4)$$

where u and w are the perturbation velocities in the x and z directions, respectively; π is the perturbation kinematic pressure; b is the perturbation buoyancy; U is the basic-state wind speed in the x direction; g is the gravitational acceleration; c_p is the specific heat of air at constant pressure; T_0 is the reference temperature; and ν is the coefficient of Rayleigh friction and Newtonian cooling. Following Baik (1992), the Rayleigh friction and Newtonian cooling terms are included in our nondimensional numerical model, and it is assumed that they have the same damping time scale. The buoyancy frequency N is assumed to be constant with height. Two basic-state wind profiles are considered: a uniform flow and a flow with a constant vertical wind shear up to a certain height [i.e., $U(z) = U_0 + \alpha z$ for $0 \le z \le z_s$, where U_0 is the basic-state horizontal wind speed at the surface, α is the constant vertical wind shear, and z_s is the top height of the shear layer] and a constant basic-state wind speed above that height. Schematic diagrams of the basic-state wind profile are shown in Fig. 1. The thermal forcing q is specified as

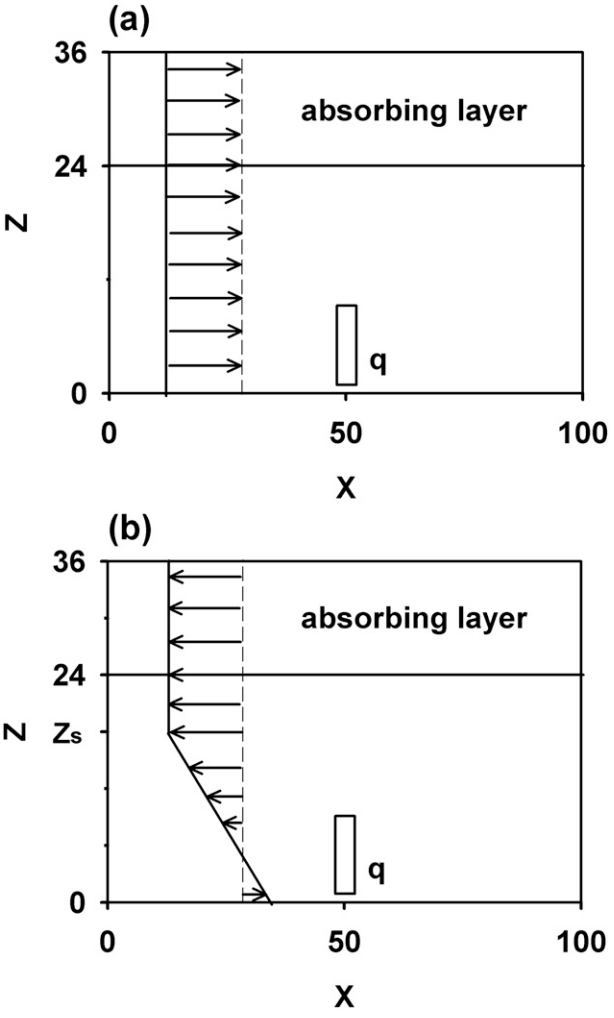

FIG. 1. Schematic diagrams of experimental design (a) in a uniform flow and (b) in a flow with a constant vertical wind shear up to a certain height (i.e., $z = z_s$) and a constant basic-state wind speed above that height.

$$q(x) = q_0 \frac{1}{[(x-c)/a_x]^2 + 1} \quad \text{for} \quad h_1 \le z \le h_2 \quad (5)$$

and represents latent heating due to deep convection. Here, q_0 is the amplitude of the thermal forcing, c is the horizontal location of the forcing center, a_x is the half-width of the bell-shaped function, and h_1 and h_2 are the forcing bottom and top heights, respectively.

The elevated heating is uniformly distributed in the vertical and is steadily applied.

Let us introduce the following dimensionless variables:

$$t = \frac{L}{U_c}\tilde{t}, \quad x = L\tilde{x}, \quad c = L\tilde{c}, \quad a_x = L\tilde{a}_x, \quad z = \frac{U_c}{N}\tilde{z}, \quad z_{\text{tr}} = \frac{U_c}{N}\tilde{z}_{\text{tr}}, \quad h_1 = \frac{U_c}{N}\tilde{h}_1,$$
$$h_2 = \frac{U_c}{N}\tilde{h}_2, \quad u = \frac{gq_0L}{c_pT_0NU_c}\tilde{u}, \quad w = \frac{gq_0}{c_pT_0N^2}\tilde{w}, \quad \pi = \frac{gq_0L}{c_pT_0N}\tilde{\pi}, \quad b = \frac{gq_0L}{c_pT_0U_c}\tilde{b}, \quad \text{and}$$
$$U = U_c\tilde{U}, \quad U_0 = U_c\tilde{U}_0, \quad \alpha = N\tilde{\alpha}, \quad q = q_0\tilde{q}, \quad \nu = \frac{U_c}{L}\tilde{\nu}, \tag{6}$$

where L is the characteristic horizontal length scale of the thermal forcing, U_c is the characteristic velocity scale of the basic-state flow, and the tilde denotes dimensionless quantities.

The nondimensional equation set is obtained by rewriting Eqs. (1)–(5) in terms of the above dimensionless variables:

$$\frac{\partial u}{\partial t} + U\frac{\partial u}{\partial x} + w\frac{dU}{dz} + \mu\left(u\frac{\partial u}{\partial x} + w\frac{\partial u}{\partial z}\right) = -\frac{\partial \pi}{\partial x} - \nu u, \tag{7}$$

$$\frac{\partial \pi}{\partial z} = b, \tag{8}$$

$$\frac{\partial b}{\partial t} + U\frac{\partial b}{\partial x} + w + \mu\left(u\frac{\partial b}{\partial x} + w\frac{\partial b}{\partial z}\right) = q - \nu b, \tag{9}$$

$$\frac{\partial u}{\partial x} + \frac{\partial w}{\partial z} = 0, \quad \text{and} \tag{10}$$

$$q(x) = \frac{1}{[(x-c)/a_x]^2 + 1} \quad \text{for} \quad h_1 \le z \le h_2, \tag{11}$$

where the tildes have been dropped for simplicity of notation. Here, μ is the nonlinearity factor of thermally induced finite-amplitude waves defined as $\mu = gq_0L/(c_pT_0NU_c^2)$ (Chun 1991; Lin and Chun 1991). If $\mu = 0$, then the nonlinear advection terms in Eqs. (7) and (9) disappear and hence the above system of equations becomes linear. As μ increases, the degree of nonlinearity of the flow system increases. The factor μ is varied from 0 to 5, and this range is determined based on Chun et al. (2008). They calculated the nonlinearity factor for various ideal and real storm cases. For ideal storm cases, the basic-state profiles of wind, temperature, and moisture and parameter values used are the same or similar to those in Weisman and Klemp (1982). For real storm cases, a case observed during the Tropical Ocean and Global Atmosphere Coupled Ocean–Atmosphere Response Experiment (TOGA COARE) on 22 February 1993 (Trier et al. 1996) and a case observed in Koto Tabang, Indonesia, on 11 April 2004 (Dhaka et al. 2005) are considered. Their results showed that the nonlinearity factor in various storm cases ranges from 0.59 to 4.53 in the presence of the basic-state wind. They also mentioned that there is no significant increase in nonlinearity factor even for convective storms with larger sizes because the heating rate averaged over a larger horizontal length scale decreases.

For the time integration, a leapfrog scheme is used with an Asselin (1972) time filter except for the first time step and the diffusion terms, which are integrated using a forward scheme. The horizontal and vertical derivatives are computed using a fourth-order compact implicit scheme (Navon and Riphagen 1979) and a centered difference scheme, respectively. A flat surface is assumed. A lateral radiation boundary condition proposed by Betz and Mittra (1992) and an upper sponge layer are considered to minimize wave reflection at boundaries. The maximum damping coefficient in the upper sponge layer is 3 for all simulations except for the shear flow case with a constant vertical wind shear, in which the maximum damping coefficient is increased to 20 to prevent the reflection of large-amplitude upward-propagating gravity waves produced in a shear flow at the top boundary. The method of Betz and Mittra (1992) is used in this study because it was found in the previous study, which used the same model (Chun et al. 2008), that the radiation boundary condition proposed by Betz and Mittra (1992) allows waves to propagate more efficiently at the lateral boundaries compared with the radiation condition proposed by Orlanski (1976). To suppress high-frequency numerical noise, a fourth-derivative diffusive filter (Perkey 1976) is employed.

The domain size is 100 in the horizontal and 36 in the vertical. The horizontal and vertical grid sizes are 0.1 and 0.05, respectively. Thus, the number of grid points is 1001×721. The time step used is 0.001, and the model is integrated up to $t = 14.4$. The upper sponge layer is located from $z = 24$ to the model top height. In this study, h_1 and h_2 are specified as 1 and 9 and correspond to dimensional heights of 1 and 9 km, respectively, for

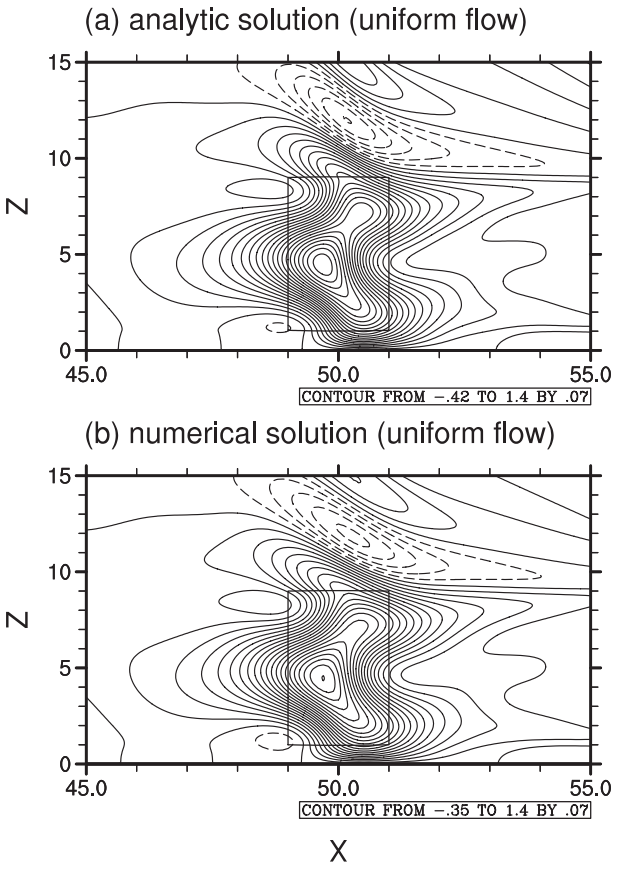

FIG. 2. The perturbation vertical velocity fields at $t = 7.2$ (a) calculated using the analytic solution given by Han and Baik (2009) and (b) simulated using the nondimensional numerical model when the nonlinear advection, Rayleigh friction, and Newtonian cooling terms are excluded (i.e., $\mu = \nu = 0$) in a uniform flow with $U = 1$. The contour interval is 0.07. The concentrated heating is located inside a small rectangle in each figure.

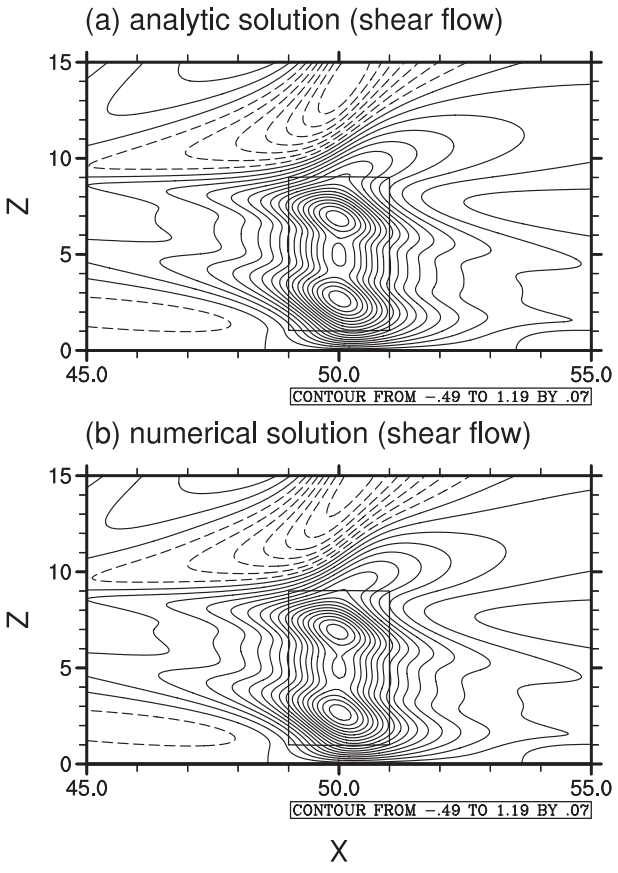

FIG. 3. The perturbation vertical velocity fields at $t = 7.2$ (a) calculated using the analytic solution given by Baik et al. (1999) and (b) simulated using the nondimensional numerical model when the nonlinear advection, Rayleigh friction, and Newtonian cooling terms are excluded (i.e., $\mu = \nu = 0$) in a shear flow with a constant vertical wind shear ($U_0 = 1.25$ and $\alpha = -0.25$, i.e., the wind reversal level is located at $z = 5$). The contour interval is 0.07. The concentrated heating is located inside a small rectangle in each figure.

$U_c = 10$ m s^{-1} and $N = 0.01$ s^{-1}. The forcing center is located at the center of the domain, and $a_x = 1$ in all numerical experiments.

3. Results and discussion

Before conducting nonlinear numerical experiments, the nondimensional model is validated by comparing the numerical solutions of a linear, inviscid flow system with the analytic solutions. Figures 2 and 3 show the vertical velocity fields calculated using the analytic solution and simulated using the nondimensional numerical model in a uniform flow and a shear flow, respectively, when the nonlinear advection, Rayleigh friction, and Newtonian cooling terms are excluded (i.e., $\mu = \nu = 0$). It is assumed that in the uniform flow case, the westerly basic-state wind exists at all heights; however, in the shear flow case, the basic-state wind blows from the west below $z = 5$ and changes its direction above that height. Both fields of stationary gravity waves in uniform and shear flows show a strong upward motion extending over the steady heating layer and alternating regions of upward and downward motion with an upstream phase tilt above the heating top. In both uniform and shear flows, a stationary gravity wave field with a slightly weaker intensity is produced above the heating top when compared to the analytic solution. Despite the small differences, the nondimensional numerical model very well reproduces the vertical velocity fields obtained analytically. In both the uniform and shear flow cases, the simulated vertical velocity fields in the heating region are remarkably similar to analytically obtained vertical velocity fields. Figures 2 and 3 indicate that the nondimensional numerical model can be used reliably to study the nonlinear effects with which we are concerned.

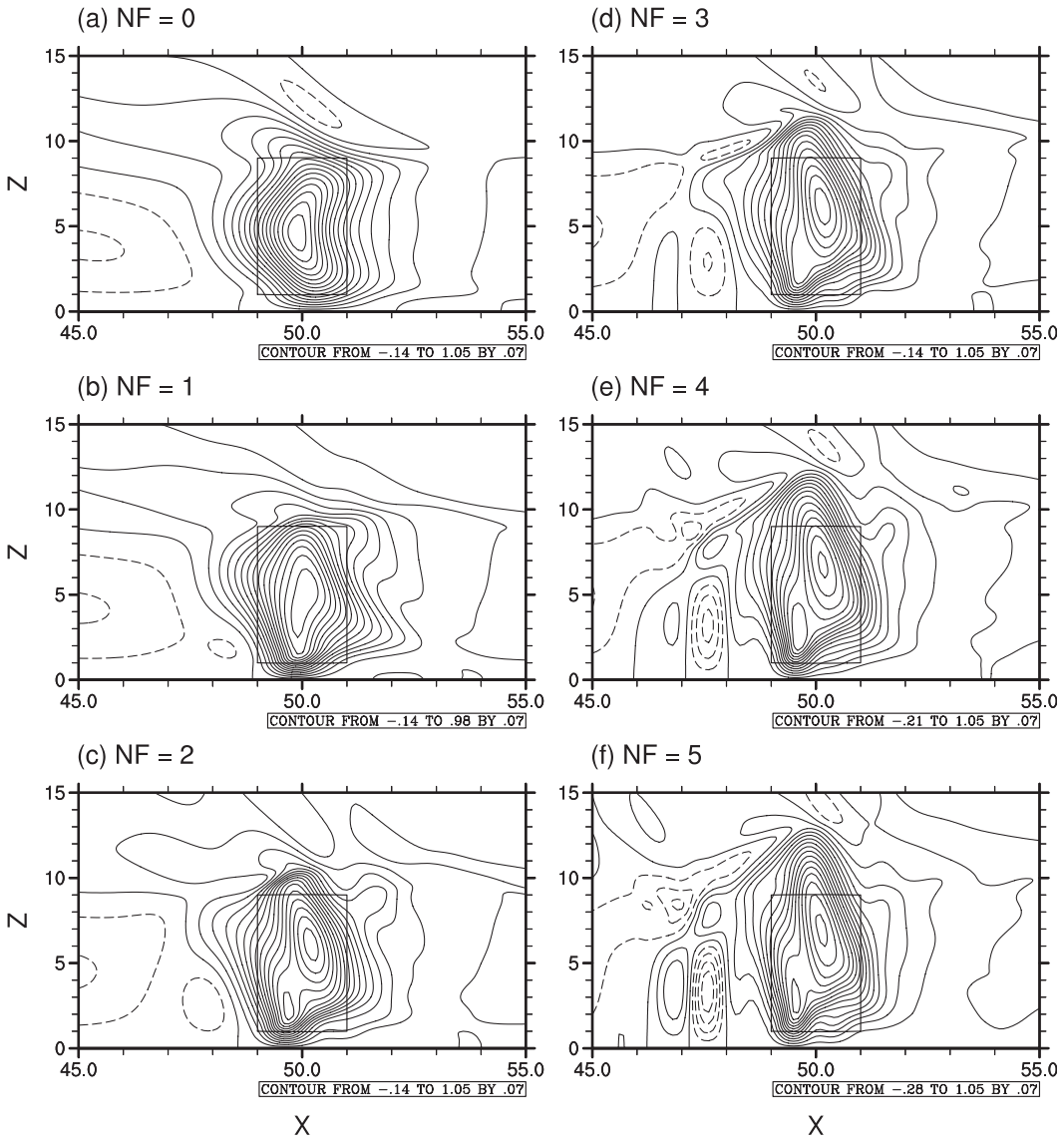

FIG. 4. The perturbation vertical velocity fields at $t = 4.2$ in a viscid, uniform flow with $\nu = 0.3$, $U = 1$, and $\mu =$ (a) 0, (b) 1, (c) 2, (d) 3, (e) 4, and (f) 5. The contour interval is 0.07.

Figure 4 shows the vertical velocity fields at $t = 4.2$ in a viscid, uniform flow with $\nu = 0.3$, $U = 1$, and various nonlinearity factors. Note that for $L = 10$ km and $U_c = 10$ m s^{-1}, $\nu = 0.3$ corresponds to a dimensional value of 0.3×10^{-3} s^{-1}. The value of ν is determined so as to obtain a quasi-steady state response field in a linear flow system. In a linear flow system (Fig. 4a), the main updraft extending over the steady heating layer has its maximum slightly below the middle of the heating layer and upwind of the heating center. In the case of $\mu = 1$ (Fig. 4b), the maximum upward motion appears slightly above the middle of the heating layer and downwind of the heating center. The low-level upward motion near and upwind of the heating center intensifies compared to that in the linear flow system. This results in a slightly intensified compensating downward motion directly upwind of that region. As the nonlinearity factor increases further (Fig. 4c), in addition to the maximum updraft that occurs in the upper-right part of the heating layer, another local maximum updraft develops in the lower-left part of the heating layer. The steady heating-induced main updraft and therefore the low-level convergence and upper-level divergence become stronger with increasing nonlinearity factor. As a result, the flow reversal region where the basic-state wind is weaker than the negative perturbation horizontal velocity

develops near the upper upwind edge of the main updraft in a uniform flow for larger nonlinearity factors ($\mu = 3$, 4, and 5). This is shown in Fig. 5 as a region where the streamlines overturn and can result in a duct between this wave-induced critical level and the surface (Clark and Peltier 1984; Baik and Chun 1996). At the same time, the compensating downdrafts develop in regions near the upper upwind edge of the main updraft and on the upwind side of the secondary maximum in the main updraft for larger nonlinearity factors (Figs. 4d–f). These compensating downdrafts help develop updrafts in regions below the compensating downdraft near the upper upwind edge of the main updraft and above the compensating downdraft upwind of the secondary maximum in the main updraft. The updraft and downdraft pairs that may be trapped in a duct propagate slowly in the upwind direction, resulting in a separation of a weak upwind cellular updraft from the main updraft region. This separation process is shown in time sequence in Fig. 6 in the case of $\mu = 5$. Figures 4 and 6 indicate that even in a uniform flow, a separation of an upwind cellular updraft from the main updraft region can occur in a highly nonlinear flow system. This is a very interesting finding. As the nonlinearity factor increases, both the height of the local maximum in the upper-right part of the heating layer and the vertical extent of the main updraft increase (Figs. 4b–f). The intensities of the upwind cellular updraft and downdraft increase with increasing nonlinearity factor. After some time, the cellular updraft and downdraft weaken as they propagate in the upwind direction. In the cases of $\mu = 3$ and 4, the cellular updraft and downdraft are eventually dissipated by viscous effects. In contrast, in the case of $\mu = 5$, the increasing nonlinear advection effect that acts to strengthen the cellular updraft and downdraft prevents the cellular updraft and downdraft from dissipating. The intensities of the cellular updraft and downdraft remain little changed, and the cellular updraft and downdraft become stationary on the upwind side.

A separation of a low-level cellular updraft from the main updraft region occurs not only on the upwind side but also on the downwind side. However, on the downwind side, it occurs regardless of whether the flow system is linear or nonlinear. The intensity of the downwind cellular updraft increases as the degree of nonlinearity of the flow system increases (not shown), but it is much weaker than that of the upwind cellular updraft in a highly nonlinear flow system (see Figs. 6c–f). In this study, we focus our analysis on the separation of a cellular updraft on the upwind side, which is a characteristic feature of a highly nonlinear flow system.

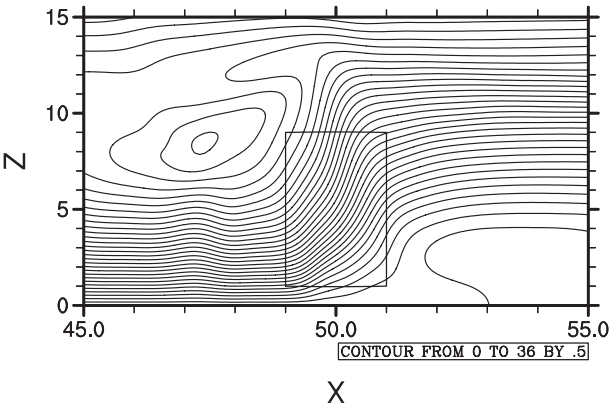

FIG. 5. The total streamfunction field at $t = 4.2$ in a viscid, uniform flow with $\nu = 0.3$, $U = 1$, and $\mu = 5$. The contour interval is 0.5.

Figure 7 shows the time series of two local updraft maxima in the main updraft region in a viscid, uniform flow for larger nonlinearity factors. The nonlinear advection results in the oscillation of the magnitude of the low-level convergence in the region below the concentrated heating region and upwind of the heating center (not shown), thus leading to the oscillatory behavior of the secondary maximum in the main updraft region. When the low-level convergence upwind of the heating center and therefore the secondary maximum updraft in the main updraft region intensify (weaken), the weak divergence above the secondary maximum and then the convergence on its downwind side are slightly intensified (weakened), thus leading to a slight increase (decrease) in the magnitude of the primary maximum in the main updraft region. As a result, the magnitudes of the two local updraft maxima exhibit decaying oscillations with a similar period but a different phase between them. The temporal maximum (minimum) of the primary maximum is produced some time after the temporal maximum (minimum) of the secondary maximum appears. The decaying amplitude is attributed to the viscous force. The oscillation period decreases as the nonlinearity factor increases (the oscillation period is about 1.8, 1.2, and 0.96 in the cases of $\mu = 3$, 4, and 5, respectively). When $\mu = 4$ and 5, there is a time range in which the secondary maximum becomes larger than the primary one. As the nonlinearity factor increases, the secondary maximum in the main updraft region and hence a separation of an upwind cellular updraft occur earlier.

The horizontal and vertical advection terms can play different roles in nonlinear processes. To understand the individual roles the horizontal and vertical advection terms play, a budget analysis of the horizontal momentum equation [Eq. (7)] and thermodynamic energy equation [Eq. (9)] is performed for the uniform flow case with $\mu = 5$. Figure 8 shows the nonlinear horizontal

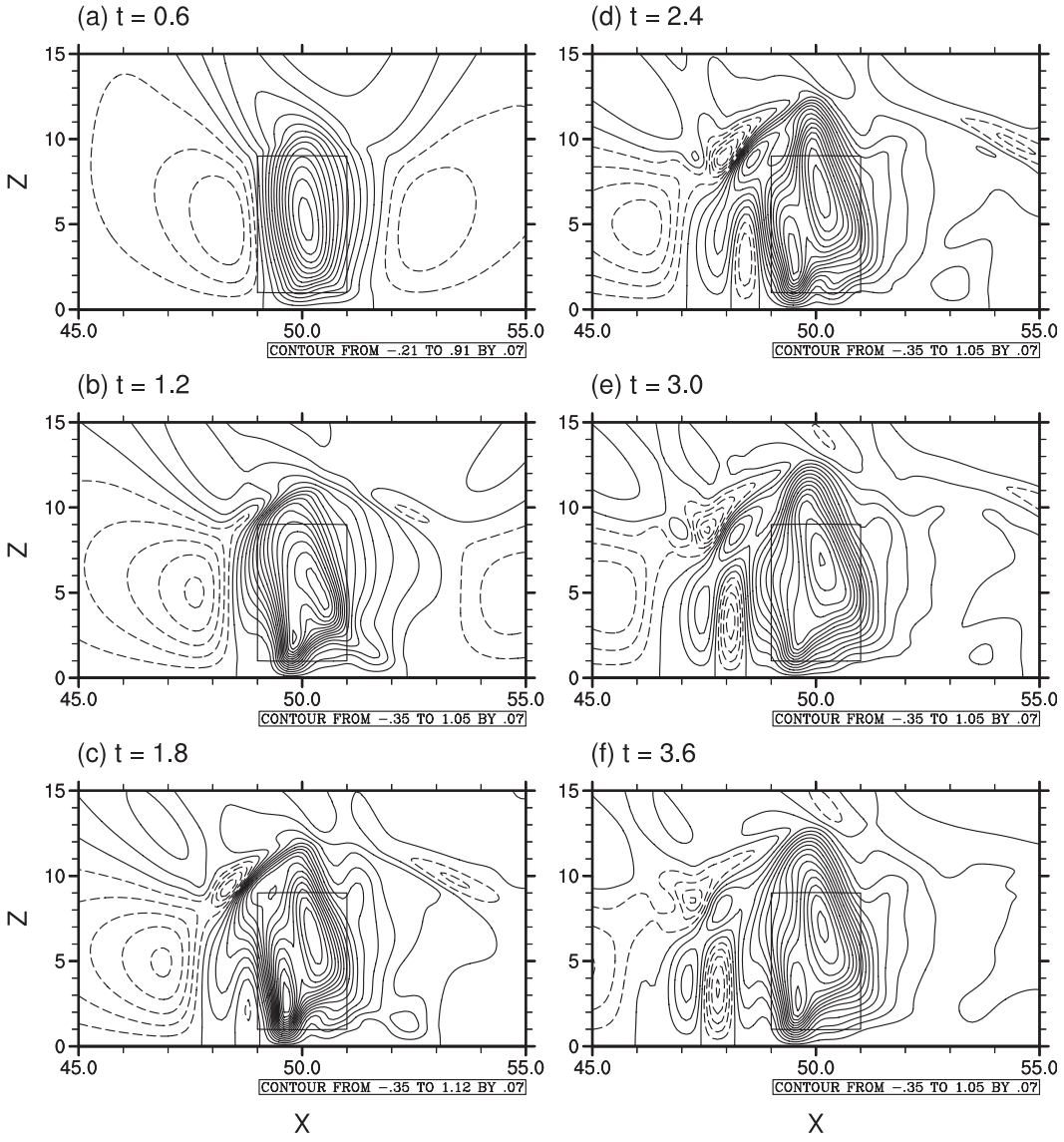

FIG. 6. The time evolution of the perturbation vertical velocity field in a viscid, uniform flow with $\nu = 0.3$, $U = 1$, and $\mu = 5$; $t =$ (a) 0.6, (b) 1.2, (c) 1.8, (d) 2.4, (e) 3.0, and (f) 3.6. The contour interval is 0.07.

advection ($-\mu u \partial u/\partial x$) and nonlinear vertical advection ($-\mu w \partial u/\partial z$) terms in the horizontal momentum equation and the nonlinear horizontal advection ($-\mu u \partial b/\partial x$) and nonlinear vertical advection ($-\mu w \partial b/\partial z$) terms in the thermodynamic energy equation at $t = 3$. The nonlinear horizontal and nonlinear vertical advection terms in the horizontal momentum equation act to weaken the lower- and upper-level westerly flow upwind of the cellular updraft, respectively. On the other hand, the nonlinear horizontal advection term in the thermodynamic energy equation acts to enhance the positive perturbation buoyancy of the cellular updraft, while the nonlinear vertical advection term acts to reduce it. Their net effect is to increase the positive perturbation buoyancy of the cellular updraft but only slightly. The orders of magnitude of the nonlinear horizontal and nonlinear vertical advection terms are similar to each other in both the horizontal momentum equation and the thermodynamic energy equation in the present two-dimensional simulation.

Viscous effects on convectively forced flows are investigated by performing numerical experiments with various coefficients of Rayleigh friction and Newtonian cooling. Figure 9 shows the Hovmöller diagram of the vertical velocity at $z = 3$ in a uniform flow with $\mu = 5$ and various coefficients of Rayleigh friction and Newtonian

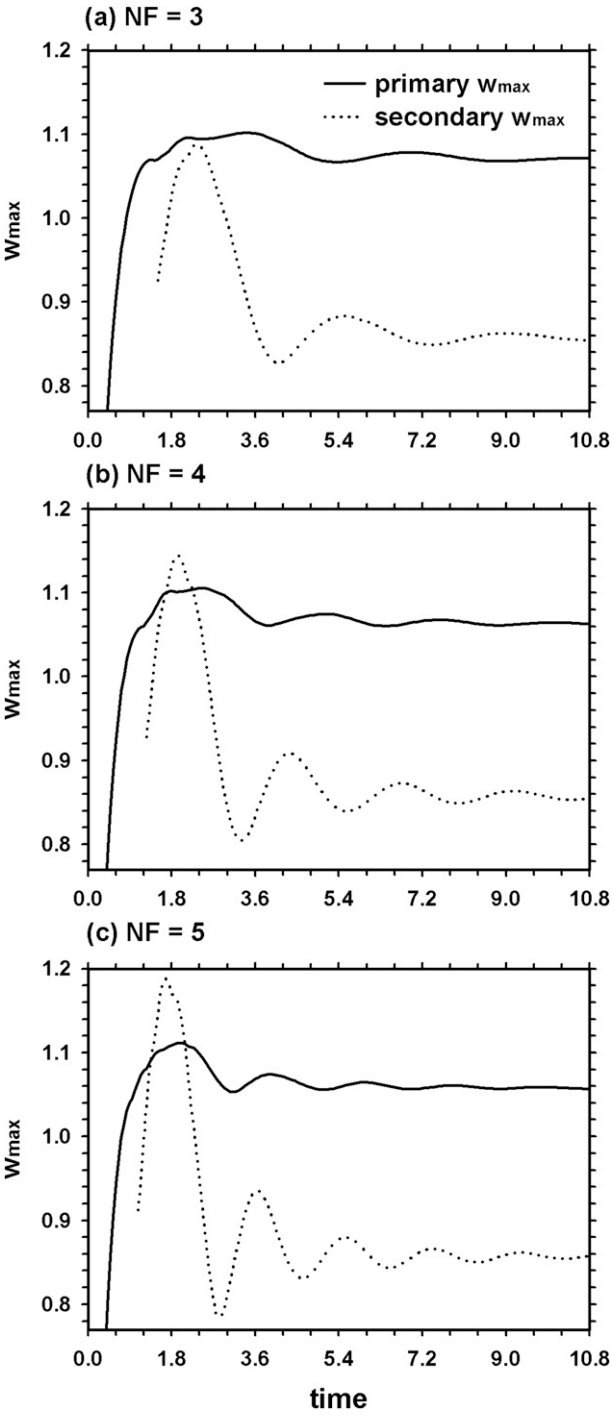

FIG. 7. The time series of two local updraft maxima in the main updraft region in a viscid, uniform flow with $\nu = 0.3$, $U = 1$, and $\mu =$ (a) 3, (b), 4, and (c) 5. To clearly show the oscillatory behavior of the two local updraft maxima, only the range of 0.77−1.2 is shown on the y axis.

cooling. In the case of $\nu = 0.3$, as already shown in Fig. 6, only one cellular updraft with a weak intensity is separated from the main updraft region on the upwind side. The cellular updraft moves slowly in the upwind direction and then becomes stationary at some distance from the heating center (Fig. 9d). With a larger coefficient ($\nu =$ 0.4), also only a single cellular updraft is separated from the main updraft, but it is eventually dissipated (Fig. 9e). In contrast, in the case of a smaller coefficient ($\nu = 0.2$), another cellular updraft with a very weak intensity is separated from the existing cellular updraft. However, unlike the existing updraft, it is dissipated after some time (Fig. 9c). When the coefficient decreases further ($\nu =$ 0.1), a new cellular updraft is separated not only from the existing cellular updraft but also from the main updraft (Fig. 9b). In the case that the viscous terms are excluded ($\nu = 0$), new cellular updrafts are periodically separated from the main updraft region after some time (Fig. 9a). As in the viscid flow shown in Fig. 7, the magnitude of the secondary maximum that occurs in the lower-left part of the main updraft region oscillates with an almost constant period. The new cellular updrafts start to be separated from the main updraft region around the time when the temporal maximum of the secondary maximum appears, while the new compensating cellular downdrafts develop around the time when the temporal minimum of the secondary maximum occurs. The separation of more cellular updrafts in a flow with a smaller ν, in which the secondary maximum maintains its large magnitude for a longer time, indicates that the secondary maximum of sufficient magnitude is necessary for the separation of an upwind cellular updraft. As ν decreases, the upwind cellular updraft and downdraft intensify further and propagate farther upwind. In particular, in an inviscid flow, the intensities of the first cellular updraft and downdraft become comparable to the intensity of the main updraft. Figure 9 indicates that the flow responses to elevated steady heating are significantly different depending on the magnitude of the coefficient of Rayleigh friction and Newtonian cooling.

The Rayleigh friction and Newtonian cooling terms can play different roles and can have different damping time scales. For simplicity, however, it is assumed in this study that the Rayleigh friction and Newtonian cooling coefficients are of equal value as in several previous studies. To understand the roles of Rayleigh friction and Newtonian cooling, additional numerical experiments were performed in which the Rayleigh friction (Newtonian cooling) coefficient is set to have different values (0, 0.1, 0.2, 0.3, and 0.4) but the Newtonian cooling (Rayleigh friction) coefficient is fixed to 0.3. Simulation results show that the Rayleigh friction plays the largest role in retarding the upwind propagation of the cellular updraft and downdraft. On the other hand, the Newtonian cooling plays the largest role in reducing the number and intensities of the cellular updraft and downdraft. From these results, it is also indirectly shown

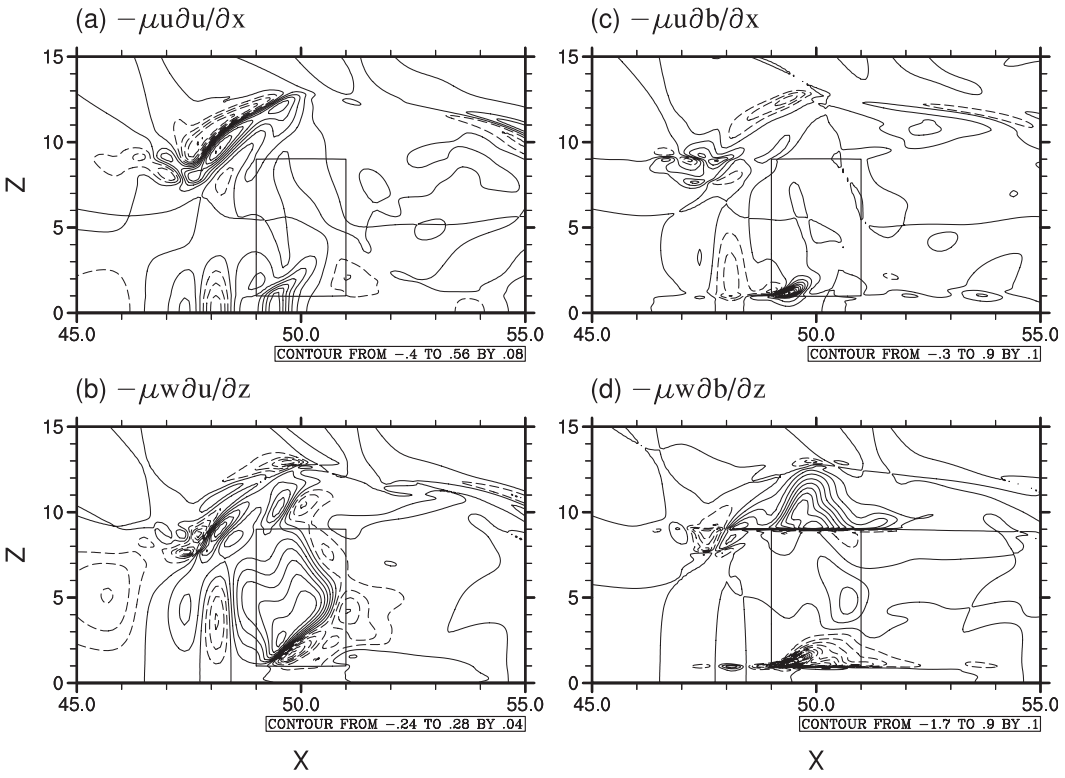

FIG. 8. The fields of (a) nonlinear horizontal advection and (b) nonlinear vertical advection in the horizontal momentum equation [Eq. (7)] and the fields of (c) nonlinear horizontal advection and (d) nonlinear vertical advection in the thermodynamic energy equation [Eq. (9)] at $t = 3$ in a viscid, uniform flow with $\nu = 0.3$, $U = 1$, and $\mu = 5$. The contour intervals are 0.08 in (a), 0.04 in (b), and 0.1 in (c),(d).

that the nonlinear momentum advection is mainly responsible for the upwind propagation of the cellular updraft and downdraft, and that the nonlinear thermal advection mainly contributes to the intensification of the cellular updraft and downdraft.

To investigate whether a change in the basic-state wind profile results in a different nonlinear response to elevated steady heating, we perform nonlinear numerical experiments in a flow with a constant vertical wind shear up to $z = z_s$ and a constant basic-state wind speed above that height (see Fig. 1b). Experimental results are shown in Fig. 10, which depicts the vertical velocity fields at $t = 3$ in a viscid flow with various nonlinearity factors. The specified parameter values are $\nu = 0.3$, $U_0 = 1.25$, $\alpha = -0.25$, and $z_s = 18$, and each corresponds to a dimensional value of 0.3×10^{-3} s^{-1}, 12.5 m s^{-1}, -2.5×10^{-3} s^{-1}, and 18 km, respectively, for $L = 10$ km, $U_c = 10$ m s^{-1}, and $N = 0.01$ s^{-1}. As in the case of uniform flow, cellular updraft and downdraft with relatively weak intensities are produced on the left side of the main updraft region for flow with large nonlinearity ($\mu = 3$, 4, and 5). As the nonlinearity factor increases, the cellular updraft and downdraft form earlier in the region closer to the main updraft region (not shown) and become stronger. The cellular updraft and downdraft in the shear flow case form farther from the main updraft region and propagate faster than those in the uniform flow case (cf. Fig. 4 with Fig. 10). The oscillatory behavior of the local updraft maxima in the main updraft region appears as in the uniform flow case, but it is irregular and its oscillation amplitude is smaller than that in the uniform flow case (not shown).

Figure 11 shows the maximum vertical velocity of the cellular updraft as a function of the Richardson number ($\mathrm{Ri} = 1/\alpha^2$). One can see that as the nonlinearity factor increases, the intensity of the cellular updraft increases for the same Ri. For a given nonlinearity factor, stronger vertical wind shear below $z = z_s$ results in more intense cellular updraft. An examination of the vertical velocity fields with various values of Ri (not shown here) indicates that the amplitude of upward-propagating gravity waves induced by the steady thermal forcing and that induced by the cellular updraft and downdraft also increase with increasing vertical wind shear.

Figure 12 shows the Hovmöller diagram of the vertical velocity at $z = 4$ with $\mu = 5$ and various values of Ri. As

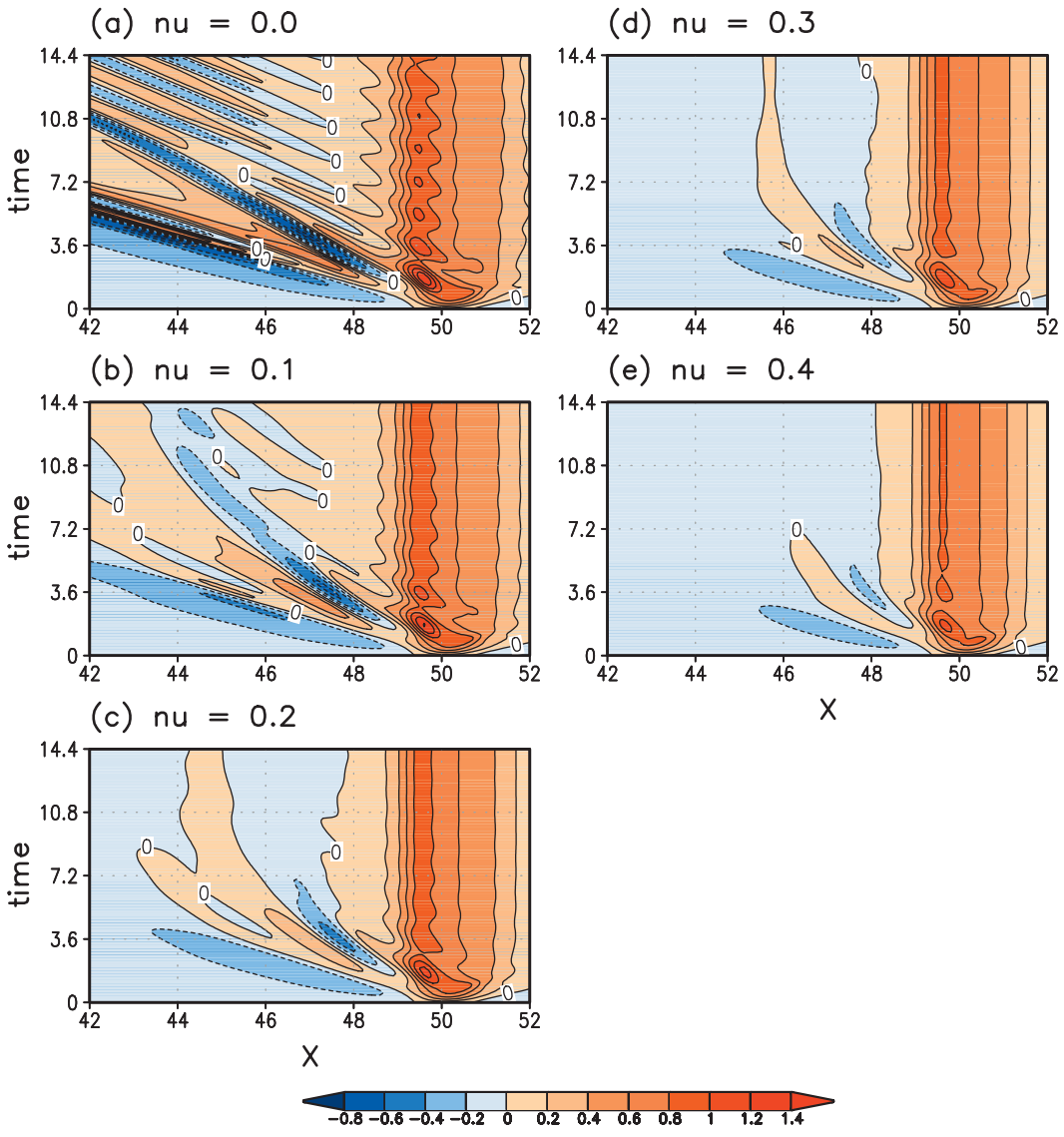

FIG. 9. The Hovmöller diagram of the perturbation vertical velocity at $z = 3$ in a uniform flow with $U = 1$, $\mu = 5$, and $\nu =$ (a) 0, (b) 0.1, (c) 0.2, (d) 0.3, and (e) 0.4. The contour interval is 0.2.

the vertical wind shear is stronger, the cellular updraft is produced earlier (not shown) and its propagation speed and longevity generally increase for the same nonlinearity factor. The propagation speed of the cellular updraft is about 2.9, 2.4, 2.1, and 2.0 and the longevity is about 8.6, 7.2, 6.4, and 6.1 in the cases of Ri = 4, 9, 16, and 25, respectively.

In the above-mentioned numerical experiments, we have used a rather simple forcing structure, which is bell shaped in the horizontal and uniform in the vertical [Eq. (11)]. Here, a realistic forcing structure resembling convective heating and cooling in squall-line systems is considered to examine the effects of nonlinearity on the flow response to squall line–type forcing. Numerous studies have been made to understand the circulation around squall lines and/or the processes responsible for repeated cell formation in squall lines (e.g., Yang and Houze 1995; Pandya and Durran 1996; Fovell and Tan 1998; Lin and Joyce 2001). Among them, Pandya and Durran (1996) demonstrated the importance of nonlinear processes by performing a linear simulation and nonlinear simulations with different amplitudes of thermal forcing. They showed that steady thermal forcing with magnitude similar to that of squall lines can produce a cellular vertical velocity field in a nonlinear simulation, as observed in actual squall lines (see their Fig. 15). The numerical model used in Pandya and Durran (1996) is a dimensional model and increasing

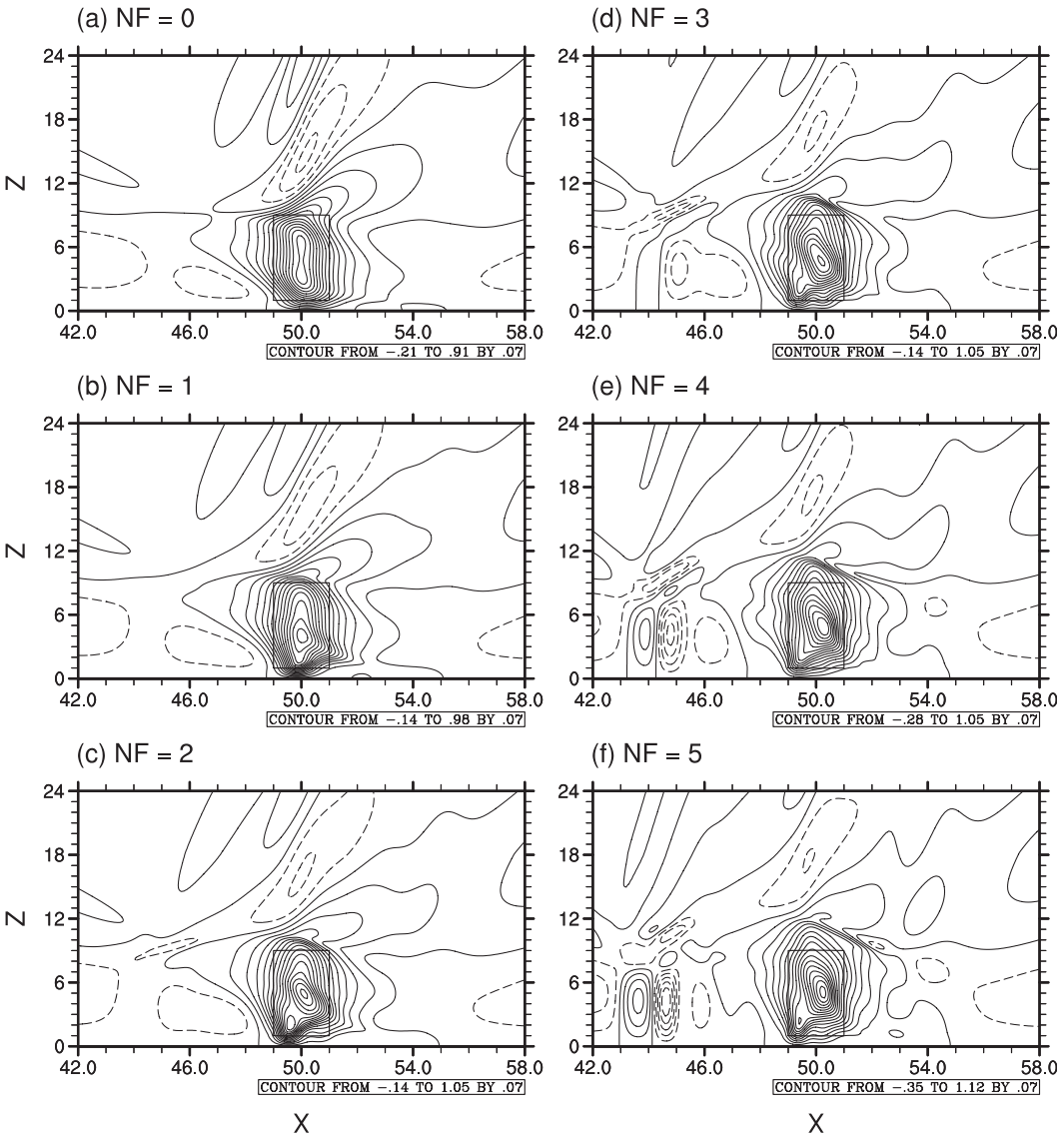

FIG. 10. The perturbation vertical velocity fields at $t = 3$ in a viscid flow corresponding to Fig. 1b with $\nu = 0.3$, $U_0 = 1.25$, $\alpha = -0.25$ (i.e., the wind reversal level is located at $z = 5$), $z_s = 18$, and $\mu =$ (a) 0, (b) 1, (c) 2, (d) 3, (e) 4, and (f) 5. The contour interval is 0.07.

the amplitude of thermal forcing implies increasing nonlinearity. In the present nondimensional model, the degree of nonlinearity of the flow system is determined not only by the amplitude of thermal forcing but also by the horizontal length scale of thermal forcing, basic-state stability, and basic-state wind speed. A combined contribution of these factors to the degree of nonlinearity is expressed by the nonlinearity factor [$\mu = gq_0L/(c_pT_0NU_c^2)$]. The squall line–type forcing used in this study is a nondimensional form of the analytic heating function of Eq. (B1) in Pandya and Durran (1996). The thermal forcing consists of leftward-tilted deep heating and low-level cooling as shown in Fig. 13.

Figure 14 shows the vertical velocity fields at $t = 14.4$ in a viscid flow with various nonlinearity factors when the squall line–type forcing exists. In these numerical experiments, the basic-state wind profile with low-level wind shear, which is typically used in squall line simulations, is considered (i.e., $U_0 = -1.8$, $\alpha = \frac{1}{3}$, and $z_s = 6$). In response to the squall line–type forcing, the flow response field in a linear flow system shows a leftward-tilted upward motion with a maximum intensity in the lower-right part of the deep heating region (Fig. 14a). In the case of $\mu = 1$, the maximum updraft becomes more confined to the region farther east (Fig. 14b). In the case of $\mu = 2$, a relatively strong cellular updraft,

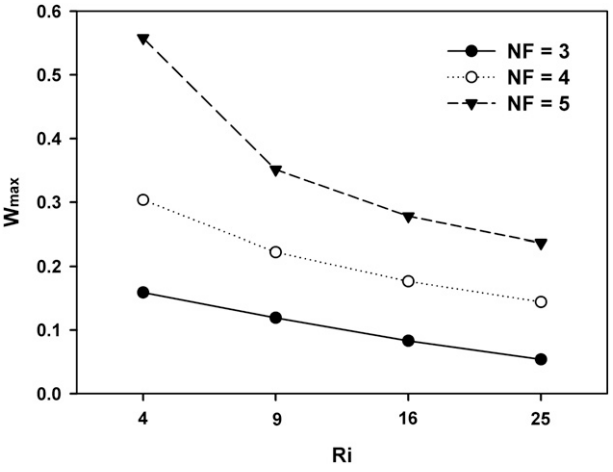

FIG. 11. The maximum vertical velocity of the cellular updraft as a function of the Richardson number in the cases of $\mu = 3$, 4, and 5. The case of Ri = 16 is the case corresponding to Fig. 10. The vertical wind shear below $z = z_s$ is varied by changing the basic-state wind speed at the surface (U_0) while maintaining the wind reversal level.

which resembles a gust front updraft observed in real squall-line systems, develops in the lower-right part of the deep heating region (Fig. 14c). When the degree of nonlinearity of the flow system increases further ($\mu = 4$ and 5), cellular updrafts are observed in and near the leftward-tilted deep heating region behind the strong leading cellular updraft (Figs. 14e,f). The intensities of these cellular updrafts increase with increasing nonlinearity factor. Figure 14 indicates that the highly nonlinear state is essential for the development of cellular updrafts. This finding is largely consistent with that of Pandya and Durran (1996), which shows that the feature of cellular vertical velocity fields in squall lines is a consequence of the nonlinear dynamics.

4. Summary and conclusions

In this study, a nondimensional numerical model was used to study the effects of nonlinearity on convectively forced mesoscale flows. In the two-dimensional numerical model, deep convective heating/cooling is specified and the nonlinearity factor μ determines the degree of nonlinearity of a flow system. It was found that a separation of an upwind cellular updraft from the steady heating-induced main updraft can occur in a highly nonlinear flow system, even without vertical wind shear. As the nonlinearity increases, the upwind cellular updraft is separated earlier and becomes more intense. For smaller viscous terms, more cellular updrafts are

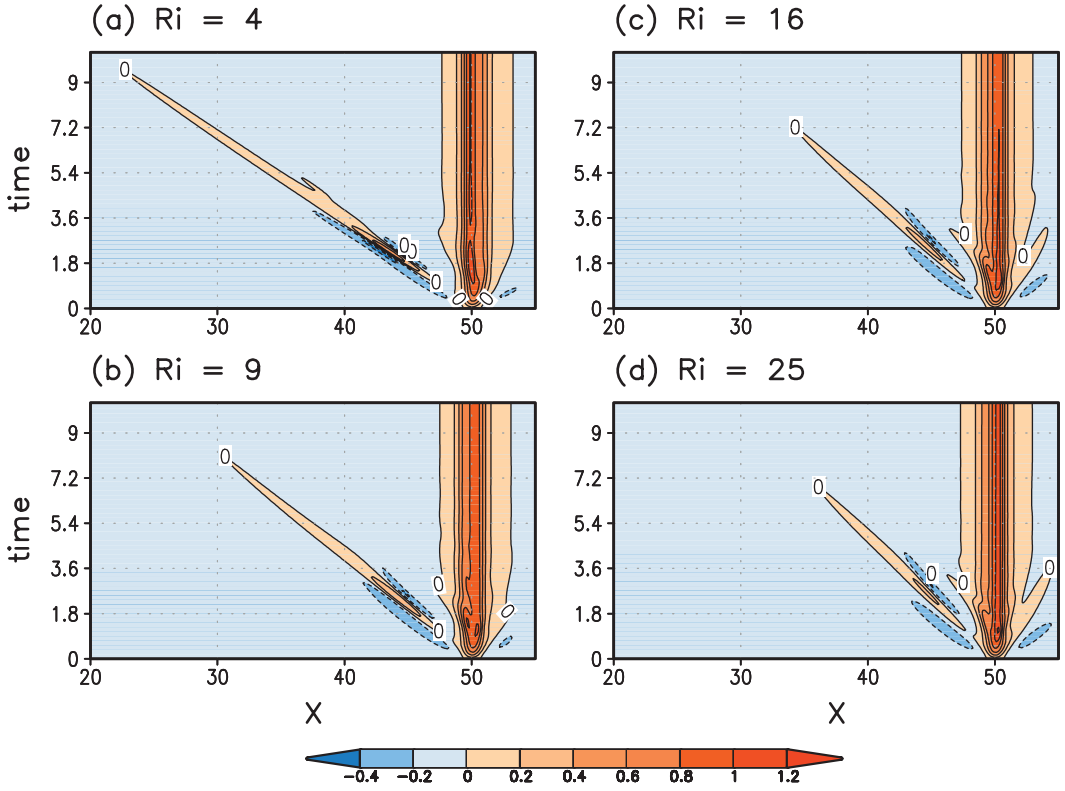

FIG. 12. The Hovmöller diagram of the perturbation vertical velocity at $z = 4$ in a viscid flow corresponding to Fig. 1b with $\nu = 0.3$, $\mu = 5$, and Ri = (a) 4, (b) 9, (c) 16, and (d) 25. The contour interval is 0.2.

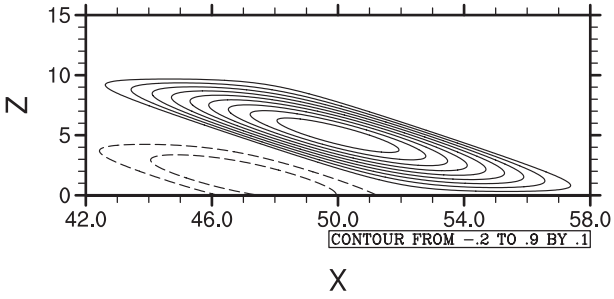

FIG. 13. The squall line–type forcing considered in this study [nondimensional form of Eq. (B1) in Pandya and Durran (1996)]. The contour interval is 0.1, and the zero contour line is not drawn.

separated from the main updraft, and they become stronger and move farther away from the main updraft region. In an inviscid flow, cellular updrafts are periodically separated from the main updraft. In a viscid flow with a constant vertical wind shear, the propagating cellular updraft and downdraft are produced when the nonlinearity is large, as in the uniform flow case. As the vertical wind shear is stronger, the cellular updraft forms earlier, is more intense, moves faster, and has a longer lifetime. Numerical experiments with squall line–type forcing indicate that the highly nonlinear state is essential for the development of cellular updrafts.

The nondimensional numerical model used in this study provided insights into the nonlinear aspects of convectively forced mesoscale flows. However, the major results obtained from our two-dimensional nonlinear simulations are applicable to mesoscale phenomena forced by two-dimensional deep convection. A further study is required to examine differences in nonlinear effects on convectively forced mesoscale flows between two- and three-dimensional simulations. In this study, the flow system is considered to be hydrostatic and the rotational effects of the Earth are neglected. It would be interesting to examine to what extent nonhydrostaticity and the Earth's rotation affect convectively forced mesoscale flows for a given degree of nonlinearity. Also, it would be interesting to examine the effects of including

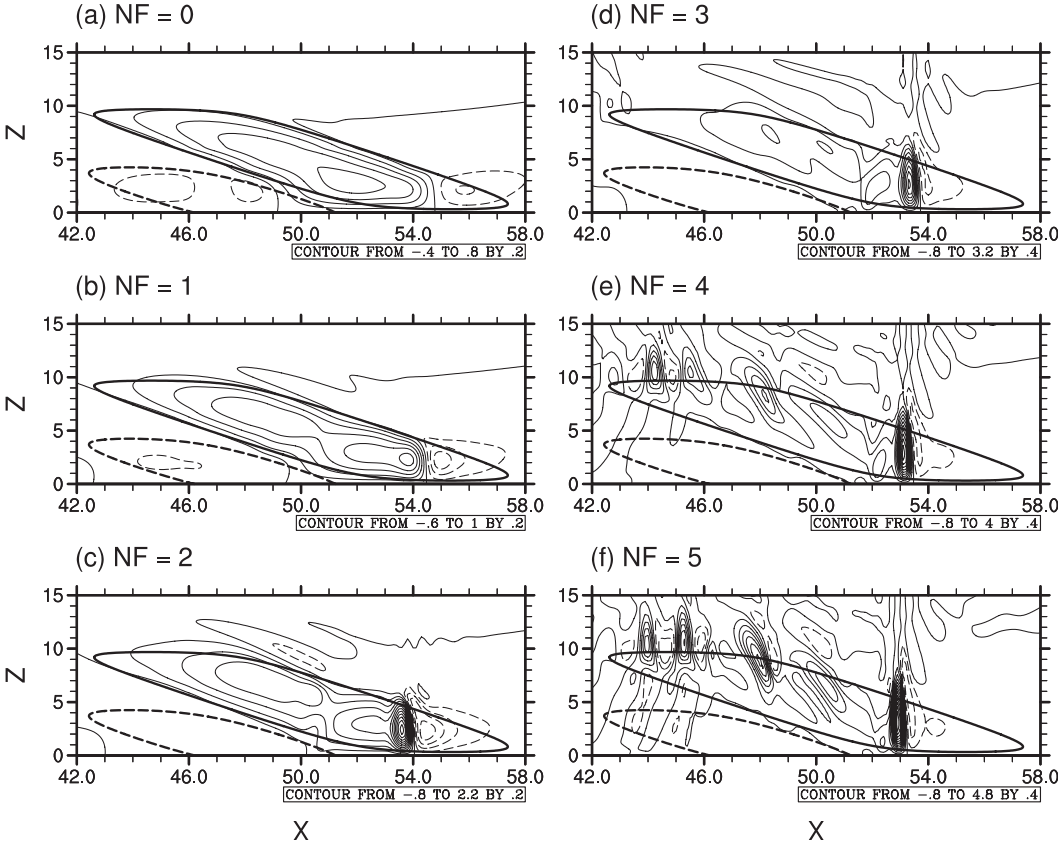

FIG. 14. The perturbation vertical velocity fields at $t = 14.4$ in a viscid flow corresponding to Fig. 1b with $\nu = 0.3$, $U_0 = -1.8$, $\alpha = 1/3$, $z_s = 6$, and $\mu =$ (a) 0, (b) 1, (c) 2, (d) 3, (e) 4, and (f) 5 when the squall line–type forcing shown in Fig. 13 exists. The contour intervals are 0.2 in (a)−(c) and 0.4 in (d)−(f). The 0.1 and −0.1 contour lines of the thermal forcing are indicated by thick solid and dashed lines, respectively.

more realistic diffusion terms (e.g., second-order diffusion terms). For these, the present nondimensional numerical model needs to be further developed. Nonlinear processes are essential for the development and maintenance of most mesoscale phenomena observed in the atmosphere. Continued research is required to better understand the nonlinear aspects of mesoscale phenomena.

Acknowledgments. The authors are grateful to anonymous reviewers for providing valuable comments on this work. This work was funded by the Korea Meteorological Administration Research and Development Program under Grant CATER 2012-6030.

REFERENCES

Asselin, R., 1972: Frequency filter for time integrations. *Mon. Wea. Rev.,* **100,** 487–490.

Baik, J.-J., 1992: Response of a stably stratified atmosphere to low-level heating—An application to the heat island problem. *J. Appl. Meteor.,* **31,** 291–303.

——, and H.-Y. Chun, 1996: Effects of nonlinearity on the atmospheric flow response to low-level heating in a uniform flow. *J. Atmos. Sci.,* **53,** 1856–1869.

——, and ——, 1997: A dynamical model for urban heat islands. *Bound.-Layer Meteor.,* **83,** 463–477.

——, H.-S. Hwang, and H.-Y. Chun, 1999: Transient, linear dynamics of a stably stratified shear flow with thermal forcing and a critical level. *J. Atmos. Sci.,* **56,** 483–499.

Betz, V., and R. Mittra, 1992: Comparison and evaluation of boundary conditions for the absorption of guided waves in an FDTD simulation. *IEEE Microwave Guided Wave Lett.,* **2,** 499–501.

Chun, H.-Y., 1991: Role of a critical level in a shear flow with diabatic forcing. Ph.D. dissertation, North Carolina State University, 159 pp.

——, 1997: Weakly non-linear response of a stably stratified shear flow to thermal forcing. *Tellus,* **49A,** 528–543.

——, and J.-J. Baik, 1994: Weakly nonlinear response of a stably stratified atmosphere to diabatic forcing in a uniform flow. *J. Atmos. Sci.,* **51,** 3109–3121.

——, H.-J. Choi, and I.-S. Song, 2008: Effects of nonlinearity on convectively forced internal gravity waves: Application to a gravity wave drag parameterization. *J. Atmos. Sci.,* **65,** 557–575.

Clark, T. L., and W. R. Peltier, 1984: Critical level reflection and the resonant growth of nonlinear mountain waves. *J. Atmos. Sci.,* **41,** 3122–3134.

Dhaka, S. K., M. K. Yamamoto, Y. Shibagaki, H. Hashiguchi, M. Yamamoto, and S. Fukao, 2005: Convection-induced gravity waves observed by the equatorial atmosphere radar (0.20°S, 100.32°E) in Indonesia. *Geophys. Res. Lett.,* **32,** L14820, doi:10.1029/2005GL022907.

Fovell, R. G., and P.-H. Tan, 1998: The temporal behavior of numerically simulated multicell-type storms. Part II: The convective cell life cycle and cell regeneration. *Mon. Wea. Rev.,* **126,** 551–577.

Grant, W., 2000: Vestibular mechanics. *The Biomedical Engineering Handbook,* J. D. Bronzino, Ed., CRC Press, 36-1–36-13.

Han, J.-Y., and J.-J. Baik, 2009: Theoretical studies of convectively forced mesoscale flows in three dimensions. Part I: Uniform basic-state flow. *J. Atmos. Sci.,* **66,** 948–966.

——, and ——, 2010: Theoretical studies of convectively forced mesoscale flows in three dimensions. Part II: Shear flow with a critical level. *J. Atmos. Sci.,* **67,** 694–712.

Lin, Y.-L., and R. B. Smith, 1986: Transient dynamics of airflow near a local heat source. *J. Atmos. Sci.,* **43,** 40–49.

——, and H.-Y. Chun, 1991: Effects of diabatic cooling in a shear flow with a critical level. *J. Atmos. Sci.,* **48,** 2476–2491.

——, and L. E. Joyce, 2001: A further study of the mechanisms of cell regeneration, propagation, and development within two-dimensional multicell storms. *J. Atmos. Sci.,* **58,** 2957–2988.

Moncrieff, M. W., 1978: The dynamical structure of two-dimensional steady convection in constant vertical shear. *Quart. J. Roy. Meteor. Soc.,* **104,** 543–567.

——, and J. S. A. Green, 1972: The propagation and transfer properties of steady convective overturning in shear. *Quart. J. Roy. Meteor. Soc.,* **98,** 336–352.

——, and M. J. Miller, 1976: The dynamics and simulation of tropical cumulonimbus and squall lines. *Quart. J. Roy. Meteor. Soc.,* **102,** 373–394.

Navon, I. M., and H. A. Riphagen, 1979: An implicit compact fourth-order algorithm for solving the shallow-water equation in conservation-law form. *Mon. Wea. Rev.,* **107,** 1107–1127.

Olfe, D. B., and R. L. Lee, 1971: Linearized calculations of urban heat island convection effects. *J. Atmos. Sci.,* **28,** 1374–1388.

Orlanski, I., 1976: A simple boundary condition for unbounded hyperbolic flows. *J. Comput. Phys.,* **21,** 251–269.

Pandya, R., and D. R. Durran, 1996: The influence of convectively generated thermal forcing on the mesoscale circulation around squall lines. *J. Atmos. Sci.,* **53,** 2924–2951.

Perkey, D. J., 1976: A description and preliminary results from a fine-mesh model for forecasting quantitative precipitation. *Mon. Wea. Rev.,* **104,** 1513–1526.

Raymond, D. J., and R. Rotunno, 1989: Response of a stably stratified flow to cooling. *J. Atmos. Sci.,* **46,** 2830–2837.

Smith, R. B., and Y.-L. Lin, 1982: The addition of heat to a stratified airstream with application to the dynamics of orographic rain. *Quart. J. Roy. Meteor. Soc.,* **108,** 353–378.

Trier, S. B., W. C. Skamarock, M. A. Lemone, D. B. Parsons, and D. P. Jorgensen, 1996: Structure and evolution of the 22 February 1993 TOGA COARE squall line: Numerical simulations. *J. Atmos. Sci.,* **53,** 2861–2886.

Weisman, M. L., and J. B. Klemp, 1982: The dependence of numerically simulated convective storms on vertical wind shear and buoyancy. *Mon. Wea. Rev.,* **110,** 504–520.

Yang, M.-J., and R. A. Houze Jr., 1995: Multicell squall-line structure as a manifestation of vertically trapped gravity waves. *Mon. Wea. Rev.,* **123,** 641–661.